Unified Solver Based Real-Time Multi-Domain Simulation of Aircraft Electro-Mechanical-Actuator

Zhen Huang ⓘ, *Student Member, IEEE*, Chengcheng Tang ⓘ, *Student Member, IEEE*,
and Venkata Dinavahi ⓘ, *Senior Member, IEEE*

Abstract—**Electro-mechanical-actuator (EMA) is the key component to convert electrical power into mechanical power for flight control in next-generation aircrafts. Multi-domain simulation of EMA can benefit its on-going evolution process. This paper presents the real-time multi-domain modeling and simulation of an EMA as elevator for flight control by utilization of a unified solver. Several key issues concerning the computational efficiency and successful implementation of this solver are provided and its relationship with state-variable model is also elaborated. Analysis shows that this solver could be a competitive candidate for multi-domain simulation because of its high computational efficiency and relatively less modeling effort. Electrical, mechanical, and thermal parts of the EMA are modeled and simulated interactively based on the proposed solver. The multi-domain model is implemented on FPGA board and executes in real time. Simulation results from FPGA board and commercial softwares under several test scenarios coincide with each other in very high degree, which showcases the efficacy of the proposed solver with respect to computational efficiency and ability to accommodate multi-domain models. The proposed model and solver are useful for hardware-in-the-loop design and testing of EMA.**

Index Terms—**Actuators, aerospace simulations, electro-mechanical systems, electro-thermal effects, real-time systems.**

I. INTRODUCTION

ELECTRO-MECHANICAL-ACTUATOR is a recently emerging concept along with the development of more electric aircraft (MEA), which is used to substitute hydraulic actuators in traditional aircraft. Its benefits are a decrease in maintenance effort and weight, and an increase in efficiency [1]. Although EMA behaves not as good as hydraulic system with respect to fault-tolerant performance, which hinders the massive use of EMAs in flight control actuators [2], it is anticipated that this barrier may be broken in the future with the development of power electronics technology with enhanced reliability. The potential to implement EMA for flight control is continually under investigation and some progress has already been made and reported [3]–[6]. Therefore, an efficient and accurate simulation

model that includes multi-domain modeling of EMA is helpful for the ongoing design and research of it.

Before a new airplane is launched into the market, numerous tests and simulations have to be done to make sure it is safe for civil flights. The recent Boeing-737 Max-8 plane crash is a negative example. It is believed to be caused by the Manoeuvring Characteristics Augmentation System (MCAS) on the plane. The MCAS was falsely triggered by the faulty signal from one of its angle of attack (α) sensors and it automatically adjusts the stabilizer to push the plane's nose down. The angle of attack can be controlled by the elevator actuator and is the key mechanical regulating variable in our multi-domain EMA model. If more comprehensive tests and simulations have been done, such tragedy could be avoided beforehand. Thus, a real-time multi-domain EMA simulation model and results will be of great value and potential for practical implementation.

Modern engineering modeling advancements and achievements have evolved many excellent tools for simulating individual aspects of an engineering problem. They can provide wide-range results in terms of accuracy and efficiency when only one kind of physical phenomenon is of concern. However, engineering problems usually involve multi-domain modeling. For example, when designing a motor drive system, not only the electrical behavior is of importance, the mechanical and thermal performance of the system should also be designed properly.

Although physical behaviors from different domains take different forms, there is one commonality: energy. Many engineering problems can be summarized in the category of energy conversion process, either within one domain (e.g. electrical energy from AC to DC by rectifier) or between two or more domains (e.g. from rotating kinetic energy to electrical energy by generator). In many cases, the energy conversion process can be described by differential-algebraic equations (DAEs).

From the mathematic point of view, as long as the physical behavior can be described by DAEs, the multi-domain simulation is no different in terms of numerical computation, regardless of the various energy forms. The solver from one physical area can be applied into another. Among some typical aspects of engineering phenomena, the electrical part usually has the smallest time-constant. The electrical transient can be as short as several microseconds or even lower to nanosecond level. That means if a unified solver for multi-domain problem is needed, the electrical system solver is most likely to be competent.

There are multiple choices for electrical system solver. The state variable method (also called state space method) is no doubt

The authors are with the Department of Electrical and Computer Engineering, University of Alberta, Edmonton, AB T6G 2R3, Canada (e-mail: zh2@ualberta.ca; ctang8@ualberta.ca; dinavahi@ualberta.ca).

Color versions of one or more of the figures in this paper are available online at http://ieeexplore.ieee.org.

a very good one. The state variables are the smallest possible subset of system variables that can represent the entire state of the system at any given time [7]. That means state variable model is a highly concise representation of the DAEs that describe the system. Consequently, the mathematic computations required for solving them are also reduced. On the other hand, it is just because of its conciseness and compactness that make the state variable model not easy to obtain. Therefore, an alternative method that can simplify the modeling process without increasing much computational burden is welcome in engineering simulation area. The Enhanced Zhen's Method (EZM) proposed in [8] achieved a good balance between modeling effort and computation effort, which makes it a suitable solver for multi-domain simulation.

As an extension of previous work in [8], this paper explores the potential to implement EZM in multi-domain simulation by an exemplary model of electro-mechanical elevator actuator for flight control on MEA. Compared with previous work, the contributions of this paper can be summarized in threefold.

1) This paper provides supplemental analysis regarding the EZM algorithm that have not been revealed before. These include how to avoid matrix inversion during the forming process of voltage/current relationship matrix $\mathbf{T}$ and how to classify voltage/current branches to avoid matrix singularity. These two issues are very important with regard to computational efficiency and successful implementation of EZM.

2) This paper provides the mathematic transformation process from EZM model to state variable model. Although it is introduced intending to illustrate the equivalence of EZM model and state variable model in mathematic modeling of circuit, it also can be viewed as a new manner to form state variable model of circuit in a way that very limited graph theory knowledge is needed.

3) For the first time in literature, the multi-domain (electrical, mechanical, thermal) modeling of EMA is introduced and solved in real-time by a unified solver in this paper. The EMA is a relatively new concept and much more research work has to be done to optimize its design. This model could be a good simulation tool to contribute to the evolution process of EMA.

II. SUPPLEMENTAL ANALYSIS OF EZM

In the modeling process of EZM, the branches of a circuit are first viewed as neither voltage or current sources and then it has been proved that for any circuit that has n nodes and b branches, the branch voltage/current relationship can be expressed in form of an anti-symmetric matrix $\mathbf{T}$ [8]. By utilization of this property, the circuit topology and component's characteristics can be decoupled and dealt with separately. As a result, the computational complexity is reduced and making EZM very suitable for parallel computing.

The antisymmetric matrix $\mathbf{T}$ is very important as it is the link between voltage and current relationships in the topology, where the current relationship can be found by manipulation of node-branch incidence matrix solely. In the forming process of

$\mathbf{T}$, one key step is to develop the voltage relationship using the following equation:

$$\mathbf{T_1} = \mathbf{A}_2'(\mathbf{A}_1')^{-1}, \qquad (1)$$

where $\mathbf{A}_1$ and $\mathbf{A}_2$ are two sections of node-branch incidence matrix $\mathbf{A}$ correspond to the n-1 voltage sources and b-n+1 current sources, respectively. The superscript $'$ denotes the transpose of a matrix.

From algorithm execution point of view, the matrix inversion should always be taken care of properly because it is usually very time consuming. This section provides a fast algorithm to compute $\mathbf{T}_1$ based on some features of $\mathbf{A}_1$, which [8] did not elaborate.

According to the definition of node-branch incidence matrix $\mathbf{A}$, there are only two non-zeros in every column, denoting the positive and negative ends' position in the topology. Moreover, one row of $\mathbf{A}$ is deleted to avoid row dependence because the sum of all rows is zero. As $\mathbf{A}_1$ is a subsection of $\mathbf{A}$, $\mathbf{A}_1$ has at most two non-zeros in each column as well and there is at least one column that has only one non-zero element.

In the proposed algorithm, the first step of computing $\mathbf{T}_1$ is performing column operations in $\mathbf{A}_1$ to eliminate one nonzero in those that have two. Take the $\mathbf{A}_1$ in [8] as an example,

$$\mathbf{A}_1 = \begin{bmatrix} 0 & 0 & 0 & 1 & 0 \\ 1 & 0 & 1 & 0 & 0 \\ -1 & 1 & 0 & 0 & 0 \\ 0 & -1 & 0 & 0 & 0 \\ 0 & 0 & 0 & 0 & -1 \end{bmatrix}. \qquad (2)$$

By subtracting column 3 from column 1 and then adding column 1 into column 2, all the columns of $\mathbf{A}_1$ have one and only one nonzero element (and it is also true for all the rows). The column operations can be represented by a series of post-multiplication of elementary matrices $\mathbf{Q}_1 \cdots \mathbf{Q}_m$, where m is the number of operations required. For $\mathbf{A}_1$ in (2),

$$\bar{\mathbf{A}}_1 = \mathbf{A}_1\mathbf{Q}_1 \cdots \mathbf{Q}_m = \begin{bmatrix} 0 & 0 & 0 & 1 & 0 \\ 0 & 0 & 1 & 0 & 0 \\ -1 & 0 & 0 & 0 & 0 \\ 0 & -1 & 0 & 0 & 0 \\ 0 & 0 & 0 & 0 & -1 \end{bmatrix}, \qquad (3)$$

where $m = 2$ and

$$\mathbf{Q}_1 = \begin{bmatrix} 1 & 0 & 0 & 0 & 0 \\ 0 & 1 & 0 & 0 & 0 \\ -1 & 0 & 1 & 0 & 0 \\ 0 & 0 & 0 & 1 & 0 \\ 0 & 0 & 0 & 0 & 1 \end{bmatrix}, \mathbf{Q}_2 = \begin{bmatrix} 1 & 1 & 0 & 0 & 0 \\ 0 & 1 & 0 & 0 & 0 \\ 0 & 0 & 1 & 0 & 0 \\ 0 & 0 & 0 & 1 & 0 \\ 0 & 0 & 0 & 0 & 1 \end{bmatrix}. \qquad (4)$$

Then the inverse of $\mathbf{A}_1$ can be written as

$$\mathbf{A}_1^{-1} = \mathbf{Q}_1 \cdots \mathbf{Q}_m\bar{\mathbf{A}}_1^{-1}. \qquad (5)$$

Note that $\bar{\mathbf{A}}_1$ has one and only one nonzero (+1 or -1) in every column and row, which makes $\bar{\mathbf{A}}_1$ an orthogonal matrix whose inverse is its transpose. The proving process is quite straightforward.

Proof: Rewrite $\bar{\mathbf{A}}_1$ into column vector form:

$$\bar{\mathbf{A}}_1 = \begin{bmatrix} \mathbf{u}_1 & \mathbf{u}_2 & \cdots & \mathbf{u}_{n-1} \end{bmatrix}, \tag{6}$$

where $\mathbf{u}_i$ are column vectors whose nonzero elements ($+1$ or -1) locate at (n-1) different rows. Then

$$\bar{\mathbf{A}}_1' \bar{\mathbf{A}}_1 = \begin{bmatrix} \mathbf{u}_1' \\ \mathbf{u}_2' \\ \cdots \\ \mathbf{u}_{n-1}' \end{bmatrix} \begin{bmatrix} \mathbf{u}_1 & \mathbf{u}_2 & \cdots & \mathbf{u}_{n-1} \end{bmatrix} = \mathbf{I}, \tag{7}$$

because

$$\mathbf{u}_i' \mathbf{u}_j = \begin{cases} 1, & \text{when} & i = j \\ 0, & \text{when} & i \neq j \end{cases}.$$

Accordingly,

$$(\mathbf{A}_1')^{-1} = (\mathbf{Q}_1 \cdots \mathbf{Q}_m \bar{\mathbf{A}}_1^{-1})' = \bar{\mathbf{A}}_1 \mathbf{Q}_m' \cdots \mathbf{Q}_1'. \tag{8}$$

Note that computing $(\mathbf{A}_1')^{-1}$ is not the ultimate goal and is not necessary. The more efficient way is combining (1) and (8) to compute $\mathbf{T}_1$ directly,

$$\mathbf{T}_1 = \mathbf{A}_2' \bar{\mathbf{A}}_1 \mathbf{Q}_m' \cdots \mathbf{Q}_1'. \tag{9}$$

As can be seen that the computation of $\mathbf{T}_1$ is split into $\mathbf{A}_2'$ post multiplication of $\bar{\mathbf{A}}_1$ and $\mathbf{Q}_m' \cdots \mathbf{Q}_1'$. Post multiplication of $\bar{\mathbf{A}}_1$ is simply reordering and sign changing of the original matrix. Post multiplication of $\mathbf{Q}_m' \cdots \mathbf{Q}_1'$ represents a series of elementary column operations that reverse to the operations from $\mathbf{A}_1$ to $\bar{\mathbf{A}}_1$. In both cases, the computation is easy to program and efficient on computer. There is no need to do matrix inversion.

Another important issue of EZM is the selection of a branch to be viewed as voltage or current source as some elements (like resistors) can be viewed as either voltage or current sources. In matrix analysis form, it's about the appropriate split of node-branch incidence matrix $\mathbf{A}$ into $\mathbf{A}_1$ and $\mathbf{A}_2$.

It can be seen in (1) that, as long as $\mathbf{A}_1$ is invertible, the subsequent analysis is valid. According to graph theory, if $\mathbf{M}(T)$ is the node-branch incidence matrix of a tree T that has n nodes, then any sub-matrix of $\mathbf{M}(T)$ of order $n-1$ is nonsingular [9]. That means, as long as the branches corresponding to $\mathbf{A}_1$ in $\mathbf{A}$ form a spanning tree, $\mathbf{A}_1$ is nonsingular. It makes sense because the branches in $\mathbf{A}_1$ should not form loops while spanning tree is a minimum subset of a graph that contains all nodes but without loops. Therefore, when selecting the branches in circuit to be deemed as voltage sources, any combination that constitutes a spanning tree of the circuit topology is practicable. The appropriate split comes from proper consideration of both topology requirements and element's characteristics. ∎

III. TRANSFORMATION BETWEEN EZM AND STATE VARIABLE MODEL

It is known that state variable method is widely accepted in many engineering areas and can be used as the tool for multi-domain simulation. However, it is challenging to analytically derive state variable models for the system with moderate to large size, thus making it inconvenient for real-time simulation. Typically speaking, some graph theory concepts like tree and
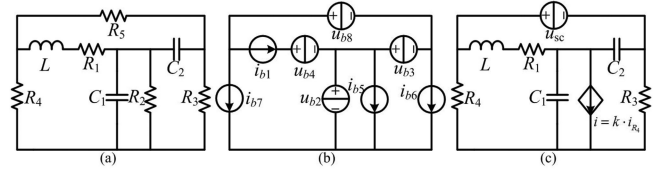

Fig. 1.   Example *RLC* network and its equivalent model in EZM.

co-tree have to be utilized for analysis [10]–[13]. This section aims at building a bridge that links state variable method and EZM, through which the state variable model of a typical circuit can be obtained by transformation from EZM model.

In the following analysis, general *RLC* circuit is considered by convention. The steps converting from EZM model to state variable model are elaborated and an example is given for better illustration, as shown in Fig. 1(a).

Step 1: Follow the routine presented in [8] to construct the EZM model and find the voltage-current relationship matrix $\mathbf{T}$. In the example given here, branch C_1, C_2, R_1 and R_5 are deemed as voltage sources while branch L, R_2, R_3 and R_4 are deemed as current sources, as shown in Fig. 1(b). The corresponding $\mathbf{T}$ matrix is as follows,

$$\begin{bmatrix} u_{b1} \\ i_{b2} \\ i_{b3} \\ i_{b4} \\ u_{b5} \\ u_{b6} \\ u_{b7} \\ i_{b8} \end{bmatrix} = \begin{bmatrix} 0 & 0 & -1 & -1 & 0 & 0 & 0 & 1 \\ 0 & 0 & 0 & 0 & -1 & -1 & -1 & 0 \\ 1 & 0 & 0 & 0 & 0 & 1 & 1 & 0 \\ 1 & 0 & 0 & 0 & 0 & 0 & 0 & 0 \\ 0 & 1 & 0 & 0 & 0 & 0 & 0 & 0 \\ 0 & 1 & -1 & 0 & 0 & 0 & 0 & 0 \\ 0 & 1 & -1 & 0 & 0 & 0 & 0 & 1 \\ -1 & 0 & 0 & 0 & 0 & 0 & -1 & 0 \end{bmatrix} \begin{bmatrix} i_{b1} \\ u_{b2} \\ u_{b3} \\ u_{b4} \\ i_{b5} \\ i_{b6} \\ i_{b7} \\ u_{b8} \end{bmatrix}. \tag{10}$$

Step 2: Write the differential equation of all energy-storage elements (inductors and capacitors) based on $\mathbf{T}$ matrix.

$$\begin{cases} u_{b1} = L \dfrac{\mathrm{d}i_{b1}}{\mathrm{d}t} = -u_{b3} - u_{b4} + u_{b8} \\[2mm] i_{b2} = C_1 \dfrac{\mathrm{d}u_{b2}}{\mathrm{d}t} = -i_{b5} - i_{b6} - i_{b7} \\[2mm] i_{b3} = C_2 \dfrac{\mathrm{d}u_{b3}}{\mathrm{d}t} = i_{b1} + i_{b6} + i_{b7} \end{cases} \tag{11}$$

Step 3: Note that it is often the case that the current of inductors and voltage of capacitors are selected as the state variables. In the above example, they are i_{b1}, u_{b2} and u_{b3}. However, the differential equations in Step 2 contain not only state variables, but also some other branch voltages and currents (called non-state variables henceforth). It is worth mentioning that the state and non-state variables constitute the complete set of branch variables used in EZM. The next operation needed is to express non-state variables in the form of state variables by taking elements' characteristics into account.

Some non-state variables have no inter-cross element with other non-state variables in matrix $\mathbf{T}$. They can be expressed as state variable forms easily. In the given example, u_{b4}, i_{b5} and

i_{b6} are such type.

$$\begin{cases} i_{b4} = \dfrac{u_{b4}}{R_1} = i_{b1} \\[2mm] u_{b5} = R_2 i_{b5} = u_{b2} \\[2mm] u_{b6} = R_3 i_{b6} = u_{b2} - u_{b3} \end{cases} \Rightarrow \begin{cases} u_{b4} = R_1 i_{b1} \\[2mm] i_{b5} = u_{b2}/R_2 \\[2mm] i_{b6} = (u_{b2} - u_{b3})/R_3 \end{cases}.$$

$$(12)$$

Other non-state variables, however, have inter-cross element with each other and matrix equation has to be solved. For i_{b7} and u_{b8} in the example, the following matrix equation can be formed,

$$\begin{cases} u_{b7} = R_4 i_{b7} = u_{b2} - u_{b3} + u_{b8} \\[2mm] i_{b8} = u_{b8}/R_5 = -i_{b1} - i_{b7} \end{cases} \Rightarrow$$

$$\begin{bmatrix} R_4 & -1 \\ 1 & 1/R_5 \end{bmatrix} \begin{bmatrix} i_{b7} \\ u_{b8} \end{bmatrix} = \begin{bmatrix} u_{b2} - u_{b3} \\ -i_{b1} \end{bmatrix}.$$

$$(13)$$

Solving (13), the remaining non-state variables are expressed in the form of state variables,

$$\begin{cases} i_{b7} = -\dfrac{R_5}{R_4 + R_5} i_{b1} + \dfrac{1}{R_4 + R_5}(u_{b2} - u_{b3}) \\[3mm] u_{b8} = -\dfrac{R_4 R_5}{R_4 + R_5} i_{b1} - \dfrac{R_5}{R_4 + R_5}(u_{b2} - u_{b3}) \end{cases}.$$

$$(14)$$

It can be observed that the matrix in this process has fixed off-diagonal elements (0 or ± 1) and only the diagonals vary with branch characteristics. Therefore, some special techniques can be utilized to expedite the solving process, such as the algorithms presented in [17].

Step 4: Combine the results in Steps 2 and 3, the differential equations can be rewritten in the form that only has state variables. The results in (11), (12) and (14) yield

$$\begin{cases} \dfrac{\mathrm{d}i_{b1}}{\mathrm{d}t} = -\left(R_1 + \dfrac{R_4 R_5}{R_4 + R_5}\right)\dfrac{1}{L} i_{b1} - \dfrac{R_5}{(R_4 + R_5)L} u_{b2} \\[4mm] \qquad\quad - \dfrac{R_4}{(R_4 + R_5)L} u_{b3} \\[4mm] \dfrac{\mathrm{d}u_{b2}}{\mathrm{d}t} = \dfrac{R_5}{(R_4+R_5)C_1} i_{b1} - \left(\dfrac{1}{R_2}+\dfrac{1}{R_3}+\dfrac{1}{R_4+R_5}\right)\dfrac{1}{C_1} u_{b2} \\[4mm] \qquad\quad + \left(\dfrac{1}{R_3}+\dfrac{1}{R_4+R_5}\right)\dfrac{1}{C_1} u_{b3} \\[4mm] \dfrac{\mathrm{d}u_{b3}}{\mathrm{d}t} = \dfrac{R_4}{(R_4+R_5)C_2} i_{b1} + \left(\dfrac{1}{R_3}+\dfrac{1}{R_4+R_5}\right)\dfrac{1}{C_2} u_{b2} \\[4mm] \qquad\quad - \left(\dfrac{1}{R_3}+\dfrac{1}{R_4+R_5}\right)\dfrac{1}{C_2} u_{b3} \end{cases},$$

$$(15)$$

which is exactly the canonical form of state variable model.

Note that it is also very convenient to handle external and dependent sources in above steps. The external sources can be viewed the same as state variables because they are permitted to appear in the right hand side of the differential equations. The only difference is that the external sources should be placed into input matrix **B** rather than system matrix **A**. The dependent

sources can be handled by putting them aside first and solving the other non-state variables. When all the other non-state variables are solved, substituting them into dependent sources' own function, then the dependent sources can be expressed as function of state variables and/or external sources as well.

In the above example, if $u_{b8} = u_{\mathrm{sc}}$ is an external stimulus voltage source and $i_{b5} = k \cdot i_{b7}$ is a current controlled current source (shown in Fig. 1.(c)), then Steps 1 and 2 of the transformation remain unchanged and the solution of non-state variables in Step 3 becomes

$$\begin{cases} u_{b4} = R_1 i_{b1} \\[2mm] i_{b6} = (u_{b2} - u_{b3})/R_3 \\[2mm] i_{b7} = (u_{b2} - u_{b3} + u_{b8})/R_4 \end{cases}.$$

$$(16)$$

Accordingly, the dependent source can be expressed as

$$i_{b5} = \frac{k}{R_4}(u_{b2} - u_{b3} + u_{b8}).$$

$$(17)$$

The corresponding state variable model of the modified schematic graph is obtained by combining (11), (16) and (17), which yield

$$\frac{d\mathbf{x}}{dt} = \mathbf{A}\mathbf{x} + \mathbf{B}u_{\mathrm{sc}},$$

$$(18)$$

where

$$\mathbf{A} = \begin{bmatrix} -\dfrac{R_1}{L} & 0 & \dfrac{1}{L} \\[4mm] 0 & -\left(\dfrac{k+1}{R_4}+\dfrac{1}{R_3}\right)\dfrac{1}{C_1} & \left(\dfrac{k+1}{R_4}+\dfrac{1}{R_3}\right)\dfrac{1}{C_1} \\[4mm] \dfrac{1}{C_2} & \left(\dfrac{1}{R_3}+\dfrac{1}{R_4}\right)\dfrac{1}{C_2} & -\left(\dfrac{1}{R_3}+\dfrac{1}{R_4}\right)\dfrac{1}{C_2} \end{bmatrix},$$

$$\mathbf{B} = \begin{bmatrix} \dfrac{1}{L} \\[3mm] -\dfrac{k+1}{R_4 C_1} \\[3mm] \dfrac{1}{R_4 C_2} \end{bmatrix}, \quad \mathbf{x} = \begin{bmatrix} i_{b1} \\[1mm] u_{b2} \\[1mm] u_{b3} \end{bmatrix}.$$

The above steps demonstrate that it is feasible to transform EZM model to state variable model. In other words, EZM model is another correct representation of mathematic description of the circuit. The state variable model and EZM model are actually one thing that takes two different forms. They are equivalent in mathematic modeling.

The effort of constructing state variable model through EZM model may not necessarily be much easier than constructing it directly using graphic theory. However, if it is for circuit simulation purpose only, there is actually no need to construct state variable model at all. The EZM model is able to offer the correct results as well. And more importantly, the effort of constructing EZM model is much easier than state variable model. The EZM takes branch variables as the computation objects and decouples them during the modeling process. It is a more natural way to comprehend the circuit and also very suitable for modeling and parallel computing on digital processors. These features
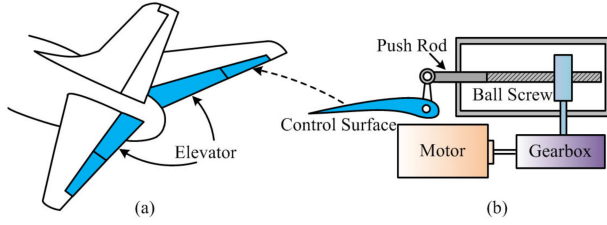
Fig. 2.   Schematic diagram of aircraft elevator and EMA.

make EZM model a competitive alternative to replace state variable model in multi-domain simulation because of its high computational efficiency and relatively less modeling effort.

IV. MULTI-DOMAIN MODELING OF ELECTRO-MECHANICAL-ACTUATOR USING EZM

This section takes electro-mechanical elevator actuator as a case study to demonstrate the fidelity of EZM serving as a tool for multi-domain simulation. The elevator in aircraft is typically located at the tail of fuselage and mainly used for pitch and altitude control, as shown in Fig. 2(a). An EMA is generally constituted of electric motor, gearbox and ball screw, as illustrated in Fig. 2(b). The push rod of EMA and the elevator surface are hinged together so as to adjust the angle of control surface. The elevator is one of the primary flight control surfaces and is very crucial for the safety and operation of aircraft [14]. Therefore, the electrical, mechanical and thermal parts of the system should be modeled and tested carefully.

A. Electrical Model

The electrical part includes complete subsections (generation, transmission and distribution) of a typical power system and also contains various conversion processes (AC to DC, DC to AC). Fig. 3(a) exhibits the structure of MEA on-board power system for EMA to be modeled in this case study. It is constituted by a synchronous generator (SG), a phase-shift transformer, two diode rectifiers, an L-C filter, a three-phase inverter and a permanent-magnet-synchronous-machine (PMSM) for driving the actuator.

Constructing the state variable model of this system is possible but very difficult and time-consuming. However, by utilization of EZM, the modeling process becomes relatively easy. Following the hierarchical and zonal decomposition process of EZM, the whole system can be split into several sub-modules according to their basic functions, as shown in Fig. 3(b). Each sub-module behaves like either current or voltage source at the output terminal to interface with other modules. The top-level solver is only responsible for the voltage-current relations between these modules and does not need to consider their internal structures. In other words, any sub-module model that conforms to the output regulation would fit for the top-level solver, from the simplest functional model to the most sophisticated device-level model.

Take the three-phase inverter module as an example, it behaves like a current source when interfacing with the L-C filter
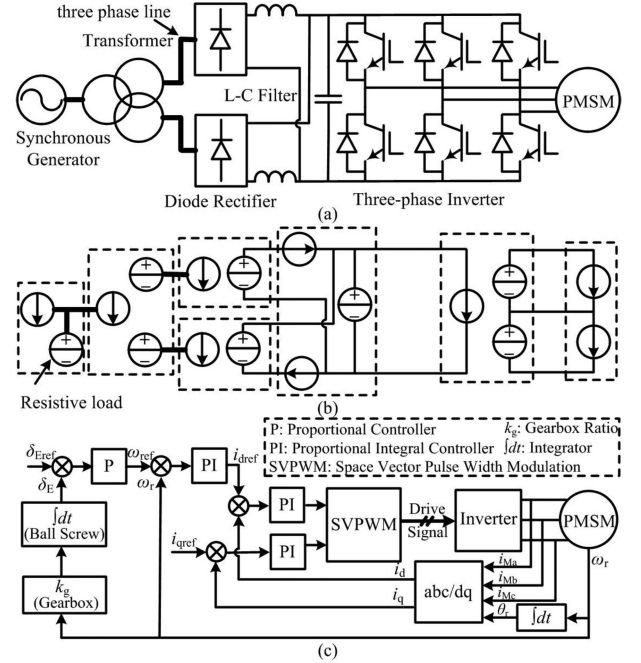

Fig. 3.   MEA on-board power system for EMA. (a) System configuration; (b) equivalent EZM model; (c) structure of control system.

and like a three-terminal-two-independent-voltage source when interfacing with the PMSM, while the L-C filter and PMSM feeds it back with their voltage and current values, respectively. The functional model adds two PMSM line currents as the value of output current source and selects 0 or ± 1 times filter voltage as the values of output voltage sources according to the switching signals from the control system. The device-level model, however, takes into account the switching transient of the power electronic devices so that the output current and voltage are no longer simple algebraic functions of the input values. This model can be realized by viewing the switches as current source in turn-off transients and steady off-state and as voltage source in turn-on transients and steady on-state.

Detailed mathematic models of the individual subsystems can be found in the following references: SG and PMSM models in [15]; diode rectifier model in [16]; insulated-gate-bipolar-transistor (IGBT) and converter model in [17] and [18]. Correspondingly, the implementation details of control scheme can be found in [5].

All the components in the circuit are viewed as either current or voltage sources under EZMs modeling principle. After proper classification and selection, the voltage/current relation of these components can be found using equation (1)–(9) and the anti-symmetry property proved in [8]. When voltage/current relation is found, the simulation process of every individual component is decoupled into two interleaved process: advancing system variable according to components characteristics and taking into account the reponse of system network. EZM does not have any specific requirement on how the component is modeled. As long as its characteristics can be described by voltage/current equations, it will fit in EZMs modeling process seamlessly.

X,Y,Z are longitudinal, transverse and vertical forces
L,M,N are roll, pitch and yaw moments

U,V,W are the forward, side and yawing velocities
Φ,Θ,Ψ are roll, pitch and yaw angles
P,Q,R are roll, pitch and yaw rates

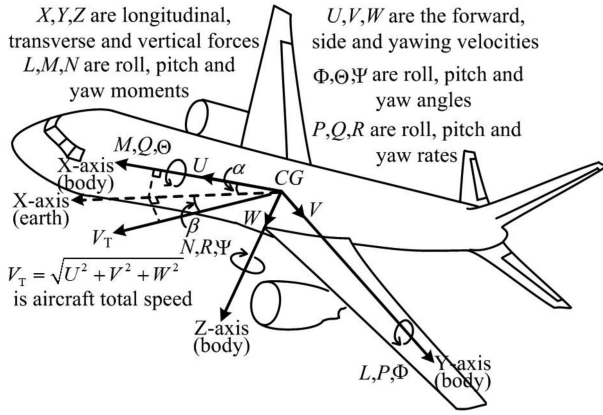$V_T = \sqrt{U^2 + V^2 + W^2}$ is aircraft total speed

Fig. 4. Definition of kinetic analysis system for aircraft with reference to body axis.

For example, the usual model of motor in [15] is a current (or flux) as state variable, voltage as stimulating source model, thus it will be modeled as current source in EZM and using the network response voltage to update its states. There is no specific restriction on its internal equations.

Another alteration of the EZM model that should be noticed is the resistive load added between the SG and the transformer. It is a common configuration that can be found in many models developed by various simulation softwares. Some softwares provide the explanation: for example, Matlab/Simulink explains it in this way: electrical machines cannot be connected to an inductive network unless a parasitic resistive or capacitive element is connected at machine terminals to avoid numerical oscillations [19]. However, this can be explained in another way from the point view of EZM modeling. It is known that inductive branches should be viewed as current sources under the EZM modeling principle, which is true for both SG and transformer windings. However, current source branches should not be connected in series to avoid circuit contention. The simplest way to resolve this contention is to add a branch between them that can be treated as voltage source, which is exactly what the resistive load is used for (approximate 5% of the machine nominal power is sufficient).

B. Mechanical Model

The mechanical analysis for aircraft flight control is usually conducted under the body-fixed axis, where the origin is located at the center of gravity (CG) of the aircraft body, as depicted in Fig. 4.

Applying the rigid-body kinetic analysis for the aircraft body, the following dynamical equations can be developed,

$$
\begin{cases}
m(\dot{U} + QW - RV + g\sin\Theta) = X \\
m(\dot{V} + UR - WP - g\cos\Theta\sin\Phi) = Y \\
m(\dot{W} + VP - QU - g\cos\Theta\cos\Phi) = Z \\
I_x\dot{P} - I_{xz}(PQ + \dot{R}) + (I_z - I_y)QR = L \\
I_y\dot{Q} - I_{xz}(P^2 - R^2) + (I_x - I_z)PR = M \\
I_z\dot{R} - I_{xz}(QR - \dot{P}) + (I_y - I_x)PQ = N
\end{cases}
\quad (19)
$$

where m is aircraft mass, g is gravity constant, I is inertia with the corresponding axis or plane indicated at its subscript. Solving (19) directly is very difficult because it is a multi-variable non-linear system. To simplify the problem, usually an equilibrium is selected and the state is written as the sum of a constant (nominal value) and a deviation (perturbation) so that the system becomes linear on a small-signal scale. Further more, the longitudinal and lateral mode analysis can be decoupled because the fuselage is slender and U is much larger than V and W. In this paper, only the longitudinal mode analysis is of interest because the elevator has negligible effect on lateral mode control.

Based on the above simplification, the small-signal linearized longitudinal equations can be written as

$$
\begin{cases}
m(\dot{u} + Q_0 w + W_0 q + g\cos(\Theta_0)\theta) = \delta X \\
m(\dot{w} - U_0 q - Q_0 u + g\sin(\Theta_0)\cos(\Phi_0)\theta) = \delta Z \\
I_y\dot{q} = \delta M \\
\dot{\theta} = q
\end{cases}
\quad (20)
$$

where the prefix δ and the lower case letters represent the deviations correspond to the upper case quantities while the subscript 0 denotes the nominal value.

On the other hand, the longitudinal perturbations of moments and forces can be expressed as the function of aerodynamic coefficients times state perturbations and control inputs [20],

$$
\begin{cases}
\delta X = \dfrac{\partial X}{\partial u}u + \dfrac{\partial X}{\partial w}w + \dfrac{\partial X}{\partial \delta_E}\delta_E + \dfrac{\partial X}{\partial \delta_T}\delta_T \\[2mm]
\delta Z = \dfrac{\partial Z}{\partial u}u + \dfrac{\partial Z}{\partial w}w + \dfrac{\partial Z}{\partial \dot{w}}\dot{w} \\[2mm]
\qquad + \dfrac{\partial Z}{\partial q}q + \dfrac{\partial Z}{\partial \delta_E}\delta_E + \dfrac{\partial Z}{\partial \delta_T}\delta_T \\[2mm]
\delta M = \dfrac{\partial M}{\partial u}u + \dfrac{\partial M}{\partial w}w + \dfrac{\partial M}{\partial \dot{w}}\dot{w} + \dfrac{\partial M}{\partial q}q \\[2mm]
\qquad + \dfrac{\partial M}{\partial \delta_E}\delta_E + \dfrac{\partial M}{\partial \delta_T}\delta_T
\end{cases}
\quad (21)
$$

where δ_e and δ_T represent the perturbations from trim in the elevator and thrust settings. The aerodynamic coefficients usually come from wind tunnel test or system identification based on experiment data [21].

Combining (20) and (21), the differential equations that describe the aircraft longitudinal stability characteristics can be obtained. The more common form is the state-variable model that uses the angle of attack α ($\tan\alpha = W/U$) to replace w as the state, which can be written as

$$
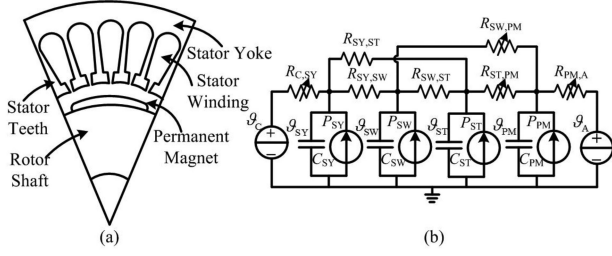\dot{\mathbf{x}} = \mathbf{A}\mathbf{x} + \mathbf{B}\epsilon,
\quad (22)
$$

Fig. 5. (a) Typical structure of PMSM; (b) equivalent lumped parameter thermal network.

Fig. 6. Functional diagram of connection between different domain models.

where

$$\mathbf{A} = \begin{bmatrix} X_u & X_\alpha & 0 & g_0\cos\theta_0 \\ Z_u & Z_\alpha & (Z_q + U_0) & g_0\sin\theta_0 \\ M_u & M_\alpha & M_q & 0 \\ 0 & 0 & 1 & 0 \end{bmatrix},$$

$$\mathbf{B} = \begin{bmatrix} X_{\delta_E} & X_{\delta_T} \\ Z_{\delta_E} & Z_{\delta_T} \\ M_{\delta_E} & M_{\delta_T} \\ 0 & 0 \end{bmatrix}, \quad \mathbf{x} = \begin{bmatrix} u \\ \alpha \\ q \\ \theta \end{bmatrix}, \quad \epsilon = \begin{bmatrix} \delta_E \\ \delta_T \end{bmatrix},$$

and

$$\begin{cases} X_u = \frac{1}{m}\frac{\partial X}{\partial u}, \dots, X_{\delta_T} = \frac{1}{m}\frac{\partial X}{\partial \delta_T} \\ Z_u = \frac{1}{m}\frac{\partial Z}{\partial u}, \dots, Z_{\delta_T} = \frac{1}{m}\frac{\partial Z}{\partial \delta_T} \\ M_u = \frac{1}{I_y}\frac{\partial M}{\partial u}, \dots, M_{\delta_T} = \frac{1}{I_y}\frac{\partial M}{\partial \delta_T} \end{cases} \quad (23)$$

C. Thermal Model

Motors should be operated without the risk for demagnetization of the magnets and/or stator winding failure [22]. The temperature rise in electric machine might exceed insulation material limit and lead to either failure of insulation or accelerated aging effect [23]. Therefore, the thermal analysis model for PMSM in the actuator system is considered in this subsection. The model is mainly adopted from [24] and will be discussed briefly here. Fig. 5 depicts the typical structure of PMSM and the equivalent lumped parameter thermal network (LPTN).

Lumped-circuit thermal model is fast in computation and have been extensively utilized and validated on numerous machine types and operating points [25]. In the adopted model, the machine is roughly divided into four parts: stator yoke, stator teeth, stator winding and permanent magnet. Each of them is represented by a node in the equivalent network and the corresponding voltages with respect to the reference (ground) $\vartheta_{SY}, \vartheta_{SW}, \vartheta_{ST}, \vartheta_{PM}$ represent the temperatures in these components. The temperatures of cooling liquid and ambient are assumed to be constant and represented by voltage sources ϑ_C, ϑ_A in the LPTN, respectively. The capacitances $C_{SY}, C_{SW}, C_{ST}, C_{PM}$ are used to model the thermal capacity of each component and the resistors are used to describe the
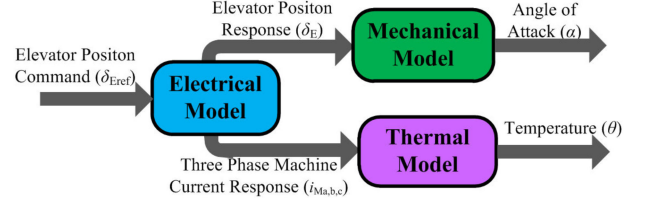
heat transfer between two components. Among the resistors, $R_{SW,SY}, R_{SW,ST}, R_{SY,ST}$ are constant because they represent the conduction heat transfer within the stationary parts, while $R_{C,SY}, R_{SW,PM}, R_{ST,PM}, R_{PM,A}$ are varying with temperature because moving parts and convection process are taken into account [24]. Thus, the thermal model is a linear parameter-varying (LPV) system and the parameters are obtained based on material and size information of PMSM as well as system identification according to experimental data. It has to mention that solving LPV system is one of the strengths of EZM because of its full decoupling nature on all circuit branches. Only matrix multiplication is involved (no matrix inversion) in EZM's computation process and it is known that the computation effort of matrix multiplication is not sensitive to parameter-varying. By proper selection and identification of these parameters, good estimation accuracy regarding the considered components can be achieved, which makes this model very suitable for on-line monitoring and protection.

V. MODEL VALIDATION

Several test scenarios are carried out to validate the fidelity of the constructed multi-domain model in this section. The reference results are obtained from commercial simulation softwares. In specific, when the model is a circuit network, it will be solved by PSCAD/EMTDC; when the model is a state variable model, it will be solved by Matlab/Simulink and the switching transients are provided by SaberRD. Obviously, the multi-domain model can not execute in real-time using these softwares. Not only because of the computation efficiency, but also that they can not communicate with each other smoothly while they are working. Therefore, PSCAD/EMTDC runs first and the results are stored in a file. Matlab/Simulink then reads this file as an input and gives the state variable results. Fig. 6 is the corresponding functional diagram showing the connection between different domain models.

The EZM model is implemented on Xilinx Virtex Ultrascale+VCU118-ES1 FPGA board to exploit its advantage of parallel computation and the 4-th order Runge-Kutta method is employed as the numerical integration method. Because the multi-domain model is solved by a unified solver, different domain models are able to communicate with each other during model execution. Thus it can be made in real-time without effort. The EZM result computed from FPGA board is exported to an digital-analog converter (DAC) along with an oscilloscope for real-time display.
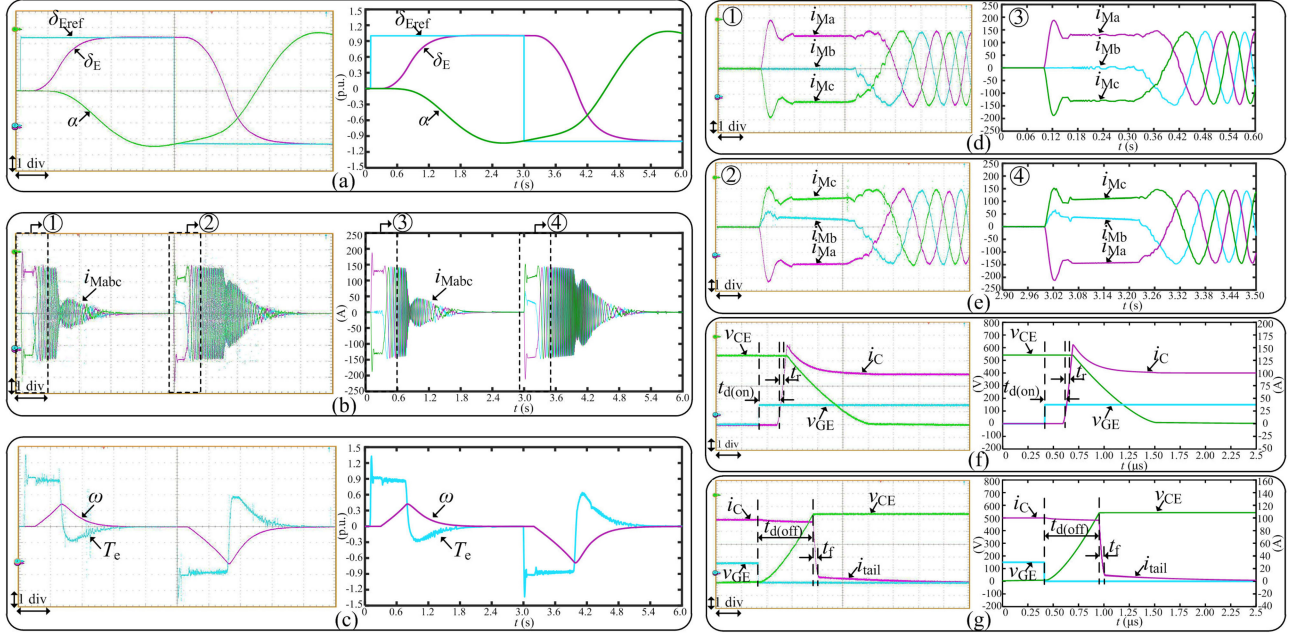
Fig. 7. Step response of the EMA system (left: EZM model; right: commercial software models). (a) Command of elevator position δ_{Eref}, responding elevator position δ_{E} and angle of attack α, y-axis: 0.3 p.u./div, x-axis: 0.6 s/div. (b) Machine three-phase currents i_{Mabc}, y-axis: 50 A/div, x-axis: 0.6 s/div. (c) Machine rotor speed ω and torque T_{e}, y-axis: 0.3 p.u./div, x-axis: 0.6 s/div. (d)~(e) Machine start-up currents i_{Mabc}, y-axis: 50 A/div, x-axis: 0.06 s/div. (f)~(g) Switching transients of power electronic devices, y-axis: 100 V/div for voltage, 25 A/div for current, x-axis: 0.25 μs/div.
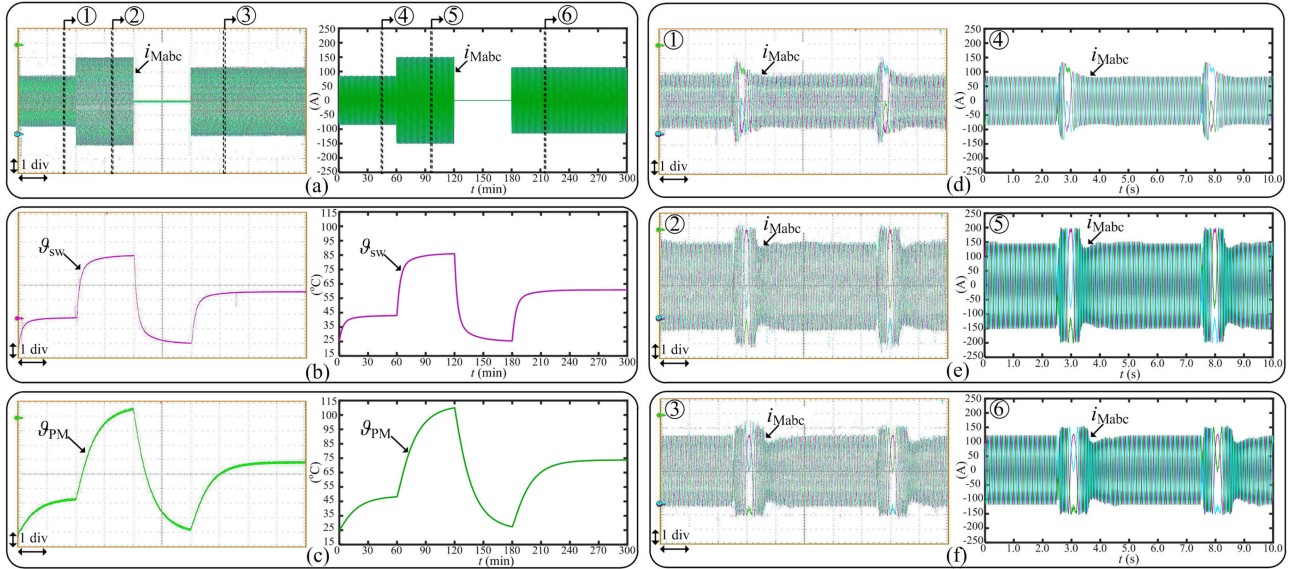

Fig. 8. Thermal test waveforms (left: EZM model; right: commercial software models). (a) Machine three-phase currents i_{Mabc}, y-axis: 50 A/div, x-axis: 30 min/div. (b) Stator winding temperature ϑ_{SW}, y-axis: 10 °C/div, x-axis: 30 min/div. (c) Permanent magnet temperature ϑ_{PM}, y-axis: 10 °C/div, x-axis: 30 min/div. (d)~(f) Snapshot of machine test currents, y-axis: 50 A/div, x-axis: 1.0 s/div.

The waveforms computed from EZM and commercial softwares are listed and compared as the following. Fig. 7 exhibits the step response of the EMA system, during which the command value of elevator position δ_{Eref} jumps from 0 to 1.0 p.u. at $t = 0.1$ s and from 1.0 to -1.0 p.u. at $t = 3.0$ s. The responding elevator position δ_{E} and resulting mechanical response of angle of attack α are illustrated in Fig. 7(a). The corresponding detailed

machine performance curves (three-phase currents i_{Mabc}, rotor speed ω and torque T_{e}) are shown in Fig. 7(b)~(c). As an important feature of EMA system, Fig. 7(d)~(e) also depict i_{Mabc} waveforms during start-up process. The actuator is initially held in position by the electric brake, and the motor must be powered before the brake is released to prevent runaway [6]. Thus, there is a period of time the machine keeps stand-still and nearly full

DC currents are induced so that high torque can be generated. Once the brake is released and the machine begin to rotate, the three-phase currents become sinusoidal. Fig. 7(f)~(g) exhibit the switching transients of power electronic devices as detailed device-level converter models are incorporated in the electrical part system. The target switching device employed in the model is Infineon FZ400R12KE4 IGBT. Turn-on and turn-off transients of IGBT are displayed and the characteristic values $t_{\mathrm{d(on)}}$, t_{r}, $t_{\mathrm{d(off)}}$, t_{f} are very close to those given in the data-sheet. It has to mention that the efficiency performance of the FPGA model and commercial software model vary greatly. To accomplish the same task in Fig. 7, PSCAD/EMTDC consumes 355.9 s, almost 60 times slower than the FPGA model, which only uses 6.0 s in real-time execution.

Fig. 8 illustrates the performance waveforms of EMA system under thermal test. The command signal δ_{Eref} given to the system is a 0.1 Hz triangle signal whose upper and lower peak are 1.0 and -1.0 p.u. respectively, which means the elevator is excited to swing back and forth to its maximum displacement position repeatedly. The ambient and cooling liquid temperatures are assumed to be 25 °C. The thermal test is conducted in four stages: (1) from 0~60 min, the load torque applied to the machine is 0.5 p.u.; (2) from 60~120 min, load torque increases to 0.9 p.u.; (3) from 120~180 min, the system is in the rest and (4) from 180~300 min, the load torque becomes 0.7 p.u. Fig. 8(a) depicts the machine currents during the four stages and Fig. 8(b)~(c) are the corresponding dynamic temperature of stator winding ϑ_{SW} and permanent magnet ϑ_{PM}, respectively. Snapshot of machine test currents in one period in stage (1), (2) and (4) are also given in Fig. 8(d)~(f). As can be seen that the larger the load torque is, the higher the temperature will be. The most serious situation occurs in stage (2) during which ϑ_{SW} becomes nearly 90 °C and ϑ_{PM} even climbs to over 100 °C. Special attention should be paid to avoid winding failure or demagnetization. Thus the system is put in rest in stage (3) to let the machine components cool down. The temperature finally stabilize in stage (4) with a safe margin from failure.

The test results provided here demonstrate that the EZM based model achieved very high agreement with commercial software models, from the fastest micro-second level switching transients all the way along to slowest minute-level thermal dynamics. It could be a good reflection of the real EMA system.

VI. Conclusion

The EMA is a promising research path for improving flight control performance in future aircraft. This paper provides a unified solver (EZM) based multi-domain simulation model of aircraft EMA system. EZM is a good alternative for modeling circuit network and has potential to be implemented in other domain engineering problems. The transformation between EZM model and state variable model is elaborated and with the help of EZM, matrix inversion can be avoided when solving a large complex system. Electrical mechanical and thermal parts of EMA system are modeled and simulated in real-time on FPGA board using this solver. The results are compared with commercial software outputs and very high consistency are achieved under several test scenarios, which demonstrate that this solver can accommodate different domain models very well. The proposed solver and EMA model could be a good HIL test-bench for EMA design and research.

Appendix

Electrical part parameters: SG capacity: 250 kVA; AC bus voltage: 230 V; DC bus voltage: ± 270 V; Switching frequency of inverter: 12 kHz; PMSM rated power: 60 kW; PMSM rated voltage: 300 V.

Mechanical part parameters: Aircraft speed: 980 km/h; Aircraft altitude: 35 000 ft; Aircraft mass: 184 000 lbs.

Thermal part parameters: C_{SY}: 5.59×10^3 J/K; C_{SW}: 2.62×10^3 J/K; C_{ST}: 2.91×10^3 J/K; C_{PM}: 1.08×10^4 J/K; $R_{\mathrm{SY,SW}}$: 0.289 K/W; $R_{\mathrm{SY,ST}}$: 0.013 K/W; $R_{\mathrm{SW,ST}}$: 0.019 K/W; $R_{\mathrm{C,SY,0}}$: 0.017 K/W; $R_{\mathrm{ST,PM,0}}$: 0.599 K/W; $R_{\mathrm{PMY,A,0}}$: 2.451 K/W; other parameters can be found in [24].

References

[1] A. Garcia, I. Cusido, J. A. Rosero, J. A. Ortega, and L. Romeral, "Reliable electro-mechanical actuators in aircraft," *IEEE Aerosp. Electron. Syst. Mag.*, vol. 23, no. 8, pp. 19–25, Aug. 2008.

[2] L. Romeral, J. A. Rosero, A. G. Espinosa, J. Cusido, and J. A. Ortega, "Electrical monitoring for fault detection in an EMA," *IEEE Aerosp. Electron. Syst. Mag.*, vol. 25, no. 3, pp. 4–9, May 2010.

[3] M. Todeschi, "Airbus-EMAs for flight controls actuation system–An important step achieved in 2011," SAE, Warrendale, PA, USA, Tech. Paper 2011-01-2732, 2011.

[4] P. Enrici, F. Dumas, N. Ziegler, and D. Matt, "Design of a high-performance multi-air gap linear actuator for aeronautical applications," *IEEE Trans. Energy Convers.*, vol. 31, no. 3, pp. 896–905, Sep. 2016.

[5] A. Trentin, P. Zanchetta, P. Wheeler, and J. Clare, "Power flow analysis in electro-mechanical actuators for civil aircraft," *IET Elect. Power Appl.*, vol. 5, no. 1, pp. 48–58, Jan. 2011.

[6] J. W. Bennett, B. C. Mecrow, A. G. Jack, and D. J. Atkinson, "A prototype electrical actuator for aircraft flaps," *IEEE Trans. Ind. Appl.*, vol. 46, no. 3, pp. 915–921, May/Jun. 2010.

[7] N. S. Nise, *Control Systems Engineering*. Hoboken, NJ, USA: Wiley, 2010.

[8] Z. Huang and V. Dinavahi, "An efficient hierarchical zonal method for large-scale circuit simulation and its real-time application on more electric aircraft microgrid," *IEEE Trans. Ind. Electron.*, vol. 66, no. 7, pp. 5778–5786, Jul. 2019.

[9] R. B. Bapat, *Graphs and Matrices*, 2nd ed. London, U.K.: Springer-Verlag, 2014.

[10] W. H. Hayt Jr., J. E. Kemmerly, and S. M. Durbin, *Engineering Circuit Analysis*, 6th ed. Boston, MA, USA: McGraw-Hill, 2002.

[11] E. S. Kuh and R. A. Rohrer, "The state-variable approach to networkanalysis," *Proc. IEEE*, vol. 53, no. 7, pp. 672–686, Jul. 1965.

[12] W. K. Durfee, M. B. Wall, D. Rowell, and F. K. Abbott, "Interactive software for dynamic system modeling using linear graphic," *IEEE Control Syst. Mag.*, vol. 11, no. 4, pp. 60–66, Jun. 1991.

[13] T. Martinez-Marin, "State-space formulation for circuit analysis," *IEEE Trans. Educ.*, vol. 53, no. 3, pp. 497–503, Aug. 2010.

[14] D. A. Caughey, "Introduction to aircraft stability and control," 2011. [Online]. Available: https://courses.cit.cornell.edu/mae5070/

[15] P. C. Krause, O. Wasynczuk, and S. D. Sudhoff, *Analysis of Electric Machinery and Drive Systems*. Piscataway, NJ, USA: Wiley, 2002.

[16] T. Yang, S. Bozhko, and G. Asher, "Functional modeling of symmetrical multipulse autotransformer rectifier units for aerospace applications," *IEEE Trans. Power Electron.*, vol. 30, no. 9, pp. 4704–4713, Sep. 2015.

[17] Z. Huang and V. Dinavahi, "A fast and stable method for modeling generalized nonlinearities in power electronic circuit simulation and its real-time implementation," *IEEE Trans. Power Electron.*, vol. 34, no. 4, pp. 3124–3138, Apr. 2019.

[18] C. Wong, "EMTP modeling of IGBT dynamic performance for power dissipation estimation," *IEEE Trans. Ind. Appl.*, vol. 33, no. 1, pp. 64–71, Jan./Feb. 1997.

[19] The Mathworks, "Simulating discretized electrical systems," 2018. [online]. Available: https://www.mathworks.com/help/physmod/sps/ powersys/ug/simulating-discretized-electrical-systems.html

[20] D. McLean, *Automatic Flight Control Systems*. Englewood Cliffs, NJ, USA: Prentice-Hall, 1990.

[21] T. I. Fossen, *Mathematic Models for Control of Aircraft and Satellites*, 3rd ed. Trondheim, Norway: Norwegian University of Science and Technology, 2013.

[22] G. D. Demetriades, H. Z. de la Parra, E. Andersson, and H. Olsson, "A real-time thermal model of a permanent-magnet synchronous motor," *IEEE Trans. Power Electron.*, vol. 25, no. 2, pp. 463–474, Feb. 2010.

[23] N. Arbab, W. Wang, C. Lin, J. Hearron, and B. Fahimi, "Thermal modeling and analysis of a double-stator switched reluctance motor," *IEEE Trans. Energy Convers.*, vol. 30, no. 3, pp. 1209–1217, Sep. 2015.

[24] O. Wallscheid and J. Böcker, "Global identification of a low-order lumped-parameter thermal network for permanent magnet synchronous motors," *IEEE Trans. Energy Convers.*, vol. 31, no. 1, pp. 354–365, Mar. 2016.

[25] A. Boglietti, A. Cavagnino, D. Staton, M. Shanel, M. Mueller, and C. Mejuto, "Evolution and modern approaches for thermal analysis of electrical machines," *IEEE Trans. Ind. Electron.*, vol. 56, no. 3, pp. 871–882, Mar. 2009.

Chengcheng Tang (S'18) received the B.S. degree in electrical engineering from North China Electric Power University, Baoding, China, in 2013 and the M.Eng. degree in biomedical engineering from Tsinghua University, Beijing, China, in 2018. She is currently working toward the Ph.D. degree with the Department of Electrical and Computer Engineering, University of Alberta, Edmonton, AB, Canada. Her research interests include modeling and simulation of more electric aircraft.

Zhen Huang (S'18) received the B.S. degree in electrical engineering from Xi'an Jiaotong University, Xi'an, China, in 2012, and the M.S. degree in electrical engineering from Tsinghua University, Beijing, China, in 2015. He is currently working toward the Ph.D. degree with the Department of Electrical and Computer Engineering, University of Alberta, Edmonton, AB, Canada. His research interests include high-performance modeling and simulation of power electronics and power systems.

Venkata Dinavahi (S'94–M'00–SM'08) received the B.Eng. degree in electrical engineering from the Visvesvaraya National Institute of Technology, Nagpur, India, in 1993, the M.Tech. degree in electrical engineering from the Indian Institute of Technology Kanpur, Kanpur, India, in 1996, and the Ph.D. degree in electrical and computer engineering from the University of Toronto, Toronto, ON, Canada, in 2000. He is currently a Professor with the Department of Electrical and Computer engineering, University of Alberta, Edmonton, AB, Canada. His research interests include real-time simulation of power systems and power electronic systems, electromagnetic transients, device-level modeling, large-scale systems, and parallel and distributed computing.